Himalayan Physics

Exploring molecular structure, electronic structure, vibrational analysis and thermal properties of Cucurbitine molecule using density functional theory

https://doi.org/10.3126/gf05x016

Prakash Poudel[1], Nirmal Bishwokarma[1], Hem Shrestha[2], Babu Ram Tiwari[3], Prakash Man Shrestha[1]*, Krishna Bahadur Rai[1]†

1 Department of Physics, Patan Multiple Campus, Lalitpur, Tribhuvan University, Nepal

2 Department of Physics, Mahendra Morang Adarsha Multiple Campus, Biratnagar, Tribhuvan University, Nepal

3 Department of Applied Sciences and Chemical Engineering, Pulchowk Campus, IOE, Tribhuvan University, Nepal

Abstract: Density functional theory (DFT) calculations were performed to investigate the structural, electronic, spectroscopic, and thermodynamic properties of the Cucurbitine molecule. All computations were carried out using the B3LYP functional with the 6-311++G(d,p) basis set implemented in the Gaussian 09 package. Geometry optimization confirmed that the molecule attains a stable minimum-energy configuration with a total energy of −12425.81 eV. The obtained HOMO–LUMO energy gap of 6.094 eV indicates high chemical stability and a hard molecular nature, which is further supported by the density of states (DOS) spectrum, exhibiting a comparable energy gap of 6.089 eV. Global reactivity descriptors were evaluated, yielding a chemical hardness of 3.047 eV, electronegativity of 3.354 eV, chemical potential of −3.354 eV, softness of 0.329 eV^{-1}, and an electrophilicity index of 2.051 eV. These descriptors provide insight into the molecule's stability, polarizability, and electron-accepting ability. Molecular electrostatic potential (MEP), electrostatic potential (ESP), and electron density analyses were performed to elucidate the charge distribution and reactive regions within the molecule. Mulliken charge analysis revealed significant charge localization, with the C3 atom carrying the highest positive charge and the C4 atom exhibiting the highest negative charge. Vibrational analysis identified the characteristic vibrational modes corresponding to C–C, C–H, C–O, C=O, C–N, O–H, and N–H bonds, showing good agreement with standard reference values. Thermodynamic parameters, including heat capacity, internal energy, enthalpy, and entropy, were found to increase with temperature, whereas the Gibbs free energy decreased, reflecting the thermal stability and energetic behavior of the Cucurbitine molecule.

Keywords: Cucurbitine molecule • Density functional theory • Electronic structures • Vibrational modes • Thermodynamic parameters

Recieved: 2026-05-01 **Revised: 2026-06-18** **Published: 2026-07-02**

* *Corresponding Author: prakash.shrestha@pmc.tu.edu.np*
† *Corresponding Author: krishna.rai@pmc.tu.edu.np*

I. Introduction

Cucurbitine ($C_5H_{10}N_2O_2$) is a naturally occurring non-proteinogenic α-amino acid primarily found in the seeds of *Cucurbitaceae* plants, including pumpkins. Its IUPAC name is *(3R)-3-Aminopyrrolidine-3-carboxylic acid*, where the *(3R)* designation refers to the chiral configuration at the third carbon of the pyrrolidine ring. The molecule contains an amino group ($-NH_2$) and a carboxylic acid group ($-COOH$) attached to the same carbon, along with a five-membered pyrrolidine ring. It was first identified in 1961 by Sun *et al.* in *Cucurbita moschata* seeds, and they investigated its biological activities and potential therapeutic applications [1]. Seeds of *Cucurbitaceae* plants have traditionally been used to treat bladder and prostate disorders, while Cucurbitine itself has been employed as an anti-allergen in pharmaceutical and cosmetic products [2]. Biochemical studies have revealed the structural and functional properties of Cucurbitine and related compounds, such as cucurbitacins, which exhibit antibacterial, antioxidant, and anticancer activities, highlighting their importance in oxidative stress regulation and disease management [3, 4]. Analytical techniques, including High-Performance Liquid Chromatography (HPLC), High-Resolution Mass Spectrometry (HRMS), Quadrupole Time-of-Flight Mass Spectrometry (QTOF-MS/MS), and ultrasonic extraction, have been employed to isolate, separate, and identify Cucurbitine, supporting its potential application as a bioactive compound in medicine and cosmetics [5–7]. Owing to its zwitterionic nature and reactive functional groups, Cucurbitine also exhibits promising applications in biomolecular design and molecular interaction studies [8]. Modification of its functional groups can significantly alter its physicochemical properties. For instance, substitution at the amino ($-NH_2$) or carboxylic acid ($-COOH$) groups may influence the highest occupied molecular orbital (HOMO)–lowest unoccupied molecular orbital (LUMO) energy gap, chemical reactivity, and molecular stability, whereas structural modifications of the pyrrolidine ring may affect charge distribution and intermolecular binding behavior [9]. Consequently, Cucurbitine derivatives may exhibit enhanced biological or chemical activity [10]. Therefore, further computational and experimental investigations, including density functional theory (DFT) calculations and molecular interaction analyses, are essential to explore their potential applications in drug design and advanced functional materials [11].

Despite these previous studies, a comprehensive and integrated theoretical investigation based on density functional theory (DFT), correlating the electronic structure, topological characteristics, non-covalent interactions, and intermolecular interactions of the Cucurbitine molecule, remains lacking. Furthermore, its detailed molecular structure, electronic properties, vibrational characteristics, and thermodynamic behavior have not been systematically explored, despite its considerable biological and pharmaceutical significance. The present study addresses this gap by providing a comprehensive DFT-based investigation of the Cucurbitine molecule, offering fundamental insights into its molecular structure, stability, and chemical reactivity that may facilitate future experimental studies and drug-development

research. Specifically, the DFT/B3LYP/6-311++G(d,p) method was employed to investigate the optimized molecular structure, reduced density gradient (RDG) and non-covalent interaction (NCI) analyses, HOMO–LUMO energy gap, global reactivity descriptors, molecular electrostatic potential (MEP), electrostatic potential (ESP), electron density (ED), density of states (DOS), Mulliken atomic charges, vibrational modes, and thermodynamic properties of the Cucurbitine molecule.

II. Computational Methodology

DFT calculations for Cucurbitine were performed using Gaussian 09W [12] with Becke's hybrid functional and the Lee–Yang–Parr correlation (B3LYP), along with the 6-311++G(d,p) basis set. The initial geometry of Cucurbitine was constructed manually using the GaussView 6.0 software [13]. B3LYP was selected for its reliable exchange-correlation treatment via hybrid Hartree–Fock and DFT contributions, ensuring accurate electronic structure predictions. The 6-311++G(d,p) basis set includes triple-zeta valence flexibility, diffuse functions (++), and polarization functions (d,p), enabling an accurate description of electron distribution, weak interactions, and molecular geometry. This combination provides a well-established balance of accuracy and computational efficiency for Cucurbitine. Using these, geometry optimization, HOMO–LUMO analysis, molecular electrostatic potential (MEP), electrostatic potential (ESP), Mulliken charges, and vibrational frequencies were computed. The density of states (DOS) was generated using GaussSum [14]. In addition, the reduced density gradient (RDG) and non-covalent interactions (NCI) were evaluated using Multiwfn software version 3.8 [15] and VMD 1.9.4a53 [16] to analyze the interactions, electron localization, and orbital localization characteristics within the molecule. Thermodynamic parameters were calculated using Moltran [17].

Global reactivity indices, including ionization potential (I), electron affinity (A), chemical potential (μ), electronegativity (χ), hardness (η), softness (S), and electrophilicity (ω), were derived from the HOMO and LUMO energies based on Koopmans' theorem [18].

$$\text{Chemical potential } (\mu) = -\frac{1}{2}(I + A) \tag{1}$$

$$\text{Electronegativity } (\chi) = \frac{1}{2}(I + A) \tag{2}$$

$$\text{Chemical hardness } (\eta) = \frac{1}{2}(I - A) \tag{3}$$

$$\text{Softness } (S) = \frac{1}{\eta} \tag{4}$$

$$\text{Electrophilicity index } (\omega) = \frac{\mu^2}{2\eta} \tag{5}$$

III. Results and Discussion

Optimized molecular geometry

Fig. 1 presents the optimized molecular geometry of the Cucurbitine molecule with its atomic symbols and atom numbering, calculated using Density Functional Theory (DFT) with the B3LYP functional and the 6-311++G(d,p) basis set. The optimized structure corresponds to the molecule's ground-state configuration, representing the lowest possible energy achieved by adjusting both electronic and nuclear coordinates. In this configuration, the molecule attains an optimized molecular geometry with an energy of −12425.81 eV.

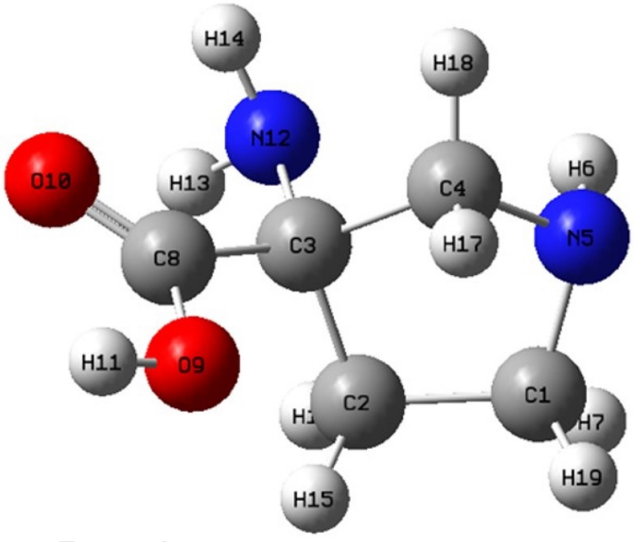

Figure 1. Optimized geometrical structure of the Cucurbitine molecule with its symbol and numbering of atoms.

The optimized molecular geometry includes bond lengths, bond angles, and dihedral angles, and the calculated structural parameters are displayed in Table 1. Bond length is determined by the bond type (e.g., hybridization and electronegativity difference), and shorter bonds are associated with higher dissociation energy and/or force constants [19]. Bond angle refers to the angle formed by three atoms separated by two bonds. Similarly, a dihedral angle is the angle produced when two planes intersect each other. The average C–C bond length is 1.507 Å [20, 21], and in Cucurbitine it ranges from 1.527–1.567 Å, showing good agreement with standard values. The C–H bond lengths are 1.0897–1.0941 Å, close to the average value of 1.09 Å [22]. The C–O and C=O bond lengths are 1.358 Å and 1.207 Å, respectively, and are in close agreement with the standard values of 1.340 Å and 1.210 Å, respectively [23]. The N–H (1.016–1.076 Å) and O–H (0.969 Å) bond lengths also lie within the reported standard ranges of 1.000–1.020 Å and 0.950–0.970 Å, respectively [24], confirming the accuracy and reliability of the optimized molecular structure.

Table 1. Optimized Bonds, Bond Length, Bond Angle and Dihedral Angle of Cucurbitine.

Bond	Value (Å)	Bond Angle	Value (°)	Dihedral Angle	Value (°)
C1–N5	1.471	O10–C8–O9	121.985	H14–N12–C3–C8	46.889
C1–H19	1.094	C8–O9–H11	107.109	H14–N12–C3–C2	174.153
C1–H7	1.091	O10–C8–C3	125.127	N12–C3–C2–H15	-143.803
C2–H15	1.090	O9–C8–C3	112.852	C3–C2–C1–H19	112.046
C2–C1	1.564	C8–C3–N12	112.236	H13–N12–C3–C2	57.354
C2–C3	1.554	C8–C3–C2	113.758	O10–C8–C3–C2	131.120
C2–H16	1.092	H13–N12–H14	106.039	O10–C8–O9–H11	-0.217
C3–C4	1.568	N12–C3–C4	107.809	C2–C4–C1–H6	73.621
C3–N12	1.462	C3–C2–H16	109.696	H13–N12–C3–C4	167.209
C3–C8	1.527	H16–C2–H15	107.967	C3–C8–O9–H11	177.699
N12–H14	1.076	H15–C2–C1	111.143	H6–N5–C1–H7	38.549
N12–H13	1.016	H17–C1–H19	107.575	C3–C4–N5–C1	-41.635
C4–H17	1.093	C2–C1–H17	112.921	C2–C1–N5–H6	-84.953
C4–H18	1.092	N5–C4–H17	109.553	C8–C3–C4–H17	40.493
C4–N5	1.457	C2–C1–H19	109.663	H15–C2–C1–H19	-8.300
N5–H6	1.016	H17–C1–N5	110.316		
C8–O10	1.207	C1–N5–H6	108.558		
C8–O9	1.358	C1–N5–C4	104.417		
O9–H11	0.969	N5–C4–H18	111.471		
		C3–C4–H18	111.964		
		C3–C4–H17	109.879		
		H18–C4–H17	108.809		
		N12–C3–C2	109.408		

Reduced density gradient and non-covalent interactions analysis

The Reduced Density Gradient (RDG) is an important approach for analyzing non-covalent interactions in molecular systems and is an effective technique for studying weak interactions such as repulsive interactions, van der Waals interactions, and hydrogen bonds. It is based on electron density and its derivatives [25], and elementary color schemes are used to distinguish each interaction. By analyzing RDG behavior and identifying weak and strong interactions based on the observed non-covalent interactions between the compound's monomer and dimer forms, this study demonstrates the stability of the molecular system. The RDG is a dimensionless quantity and is calculated by the following formula [26]:

$$\mathrm{RDG}\,(r) = \frac{1}{2(3\pi^2)^{\frac{1}{3}}} \frac{|\nabla\rho(r)|}{\rho(r)^{\frac{4}{3}}} \tag{6}$$

In the above relation, $\nabla\rho(r)$ represents the gradient of the electron density, and $\rho(r)$ represents the electron density at a specific point in space. The Reduced Density Gradient (RDG) is plotted as a function of $\mathrm{sign}(\lambda_2)\rho$, where λ_2 is the second eigenvalue of the electron density. RDG scatter plots reveal different interaction types: $\mathrm{sign}(\lambda_2)\rho > 0$ (red color) indicates steric repulsion, $\mathrm{sign}(\lambda_2)\rho < 0$ (blue color in the isosurfaces) indicates attractive interactions such as hydrogen bonds, and $\mathrm{sign}(\lambda_2)\rho \approx 0$ (green

color) indicates weak van der Waals interactions [27]. In the RDG scatter plot of Fig. 2(a) the negative sign(λ_2)ρ region shows an absence of blue spikes, indicating the absence of strong attractive interactions attributed to hydrogen bonding. The region around sign(λ_2)$\rho \approx 0$ (green) has some green spikes and corresponds to weak van der Waals interactions, mainly involving C–H contacts, while the positive region with red spikes represents steric repulsion between closely spaced atoms. The NCI isosurface plot in Fig. 2(b) supports these observations, where the absence of blue disk-like surfaces indicates the absence of strong attractive interactions. The scattered green half-disks across the molecule correspond to weak van der Waals interactions, and the red half-disks represent strong steric repulsion located within the ring-like structure and outside the ring. Although the Cucurbitine molecule contains NH_2, COOH, and OH groups that can potentially participate in hydrogen bonding, the optimized gas-phase geometry does not provide a favorable spatial arrangement for the formation of strong intramolecular hydrogen bonds. As a result, no prominent blue spikes are observed in the RDG scatter plot, indicating the absence of significant attractive hydrogen-bonding interactions within the isolated molecule. Together, these results provide a clear picture of the types and spatial distribution of interactions in the molecule.

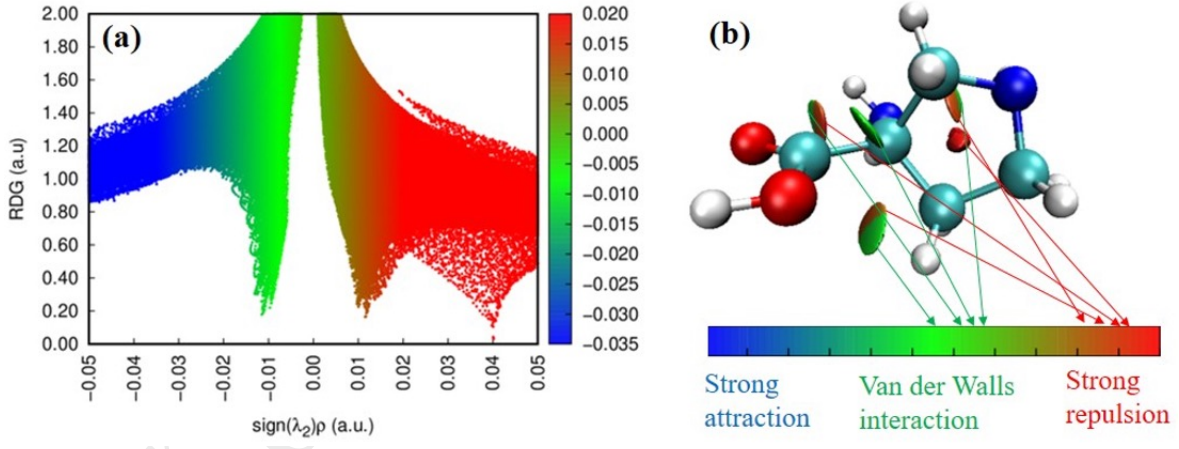

Figure 2. (a) Reduced density gradient (RDG) scatter plot, and (b) Non-covalent interaction (NCI) isosurface of the title compound.

Frontier molecular orbitals

The frontier molecular orbitals (FMOs) are the highest occupied molecular orbital (HOMO) and the lowest unoccupied molecular orbital (LUMO), and they explain a molecule's chemical stability through its energy gap. Higher HOMO energy favors electron donation, whereas lower LUMO energy enhances electron acceptance. The energy gap (HOMO–LUMO difference) indicates molecular stability and electron mobility [28]. In Fig. 3, the HOMO and LUMO energies of the Cucurbitine molecule are −6.582 eV and −0.488 eV, respectively, yielding an energy gap of 6.094 eV. The HOMO–LUMO gap of 6.094 eV indicates that the Cucurbitine molecule is highly stable and chemically less reactive. Such a large energy

gap suggests that electron excitation from the HOMO to the LUMO requires significant energy, leading to low electron mobility and insulating behavior. As a result, the molecule shows weak electron-donating and electron-accepting abilities, making it resistant to oxidation, reduction, and other chemical reactions. This implies high kinetic and thermodynamic stability along with strong structural rigidity [29]. Due to these properties, Cucurbitine may be useful in applications requiring stable molecular frameworks, such as drug design, bioactive compounds, and host–guest chemistry systems, where controlled reactivity and durability are important.

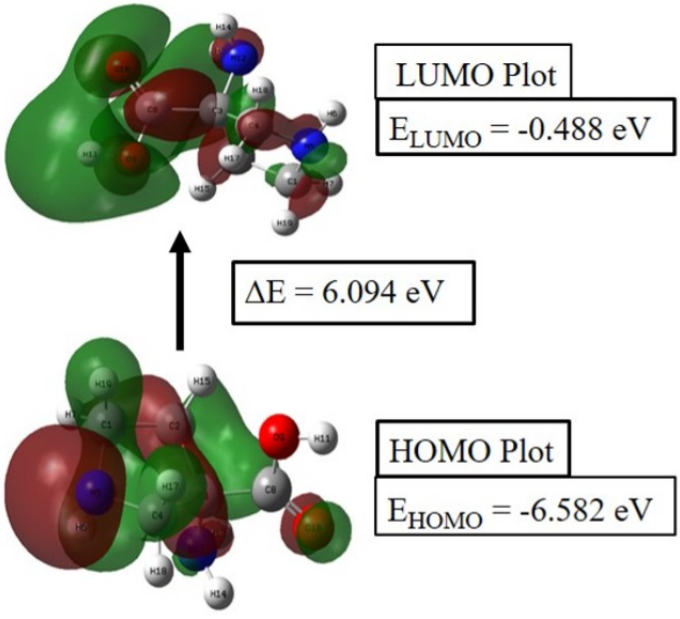

Figure 3. HOMO and LUMO distributions and the energy gap (ΔE) of the Cucurbitine molecule.

Global reactivity parameters

The global reactivity of the molecule is evaluated through the ionization potential (I) and electron affinity (A). These parameters include the chemical potential (μ), electronegativity (χ), hardness (η), softness (S), and electrophilicity index (ω), and are calculated using Eq. (1)-(5). For $C_5H_{10}N_2O_2$, the ionization potential (6.582 eV) shows a moderate ease of electron removal, while the low electron affinity (0.488 eV) indicates a weak ability to accept electrons. The negative chemical potential (μ) with a value of −3.354 eV suggests overall electronic stability with a slight tendency to attract electrons. The electronegativity (χ) (3.354 eV) reflects a moderate electron-attracting ability, whereas the high hardness (η) (3.047 eV) and low softness (S) (0.329 eV^{-1}) confirm that the molecule is stable and not highly reactive. The electrophilicity index (ω) (2.051 eV) indicates a moderate ability to accept electrons in reactions [30–32]. Overall, these values show that the molecule is chemically stable, weakly reactive, and exhibits limited donor–acceptor behavior, consistent with its large HOMO–LUMO gap (6.094 eV). The

relatively high ionization potential indicates that electron removal requires considerable energy, suggesting oxidation resistance. Likewise, the low electron affinity reflects a limited tendency to accept additional electrons. The high hardness and low softness imply strong resistance to charge transfer and low polarizability, which is consistent with the large HOMO–LUMO energy gap and enhanced kinetic stability. Furthermore, the moderate electrophilicity value suggests a moderate electron-accepting character, while the oxygen and nitrogen atoms identified from the MEP and Mulliken charge analyses may act as localized reactive sites for intermolecular interactions.

Molecular electrostatic potential, electrostatic potential, and electron density analysis

MEP illustrates the distribution of electric potential generated by a molecule's electrons and nuclei, serving as a reactivity map. Positive regions attract nucleophiles, while negative regions attract electrophiles [33–35]. In Fig. 4(a), the MEP ranges from -5.866×10^{-2} to 5.866×10^{-2} a.u., with different color coding indicating potential variation: red for electron-rich (nucleophilic) and blue for electron-deficient (electrophilic) areas. The MEP shows electrophilic and nucleophilic sites due to the unequal electron distribution arising from differences in electronegativity. Oxygen and nitrogen are electron-rich, so they act as nucleophilic sites involved in electron donation and hydrogen bonding, while hydrogen atoms are electron-deficient and act as electrophilic sites involved in proton or nucleophile interactions.

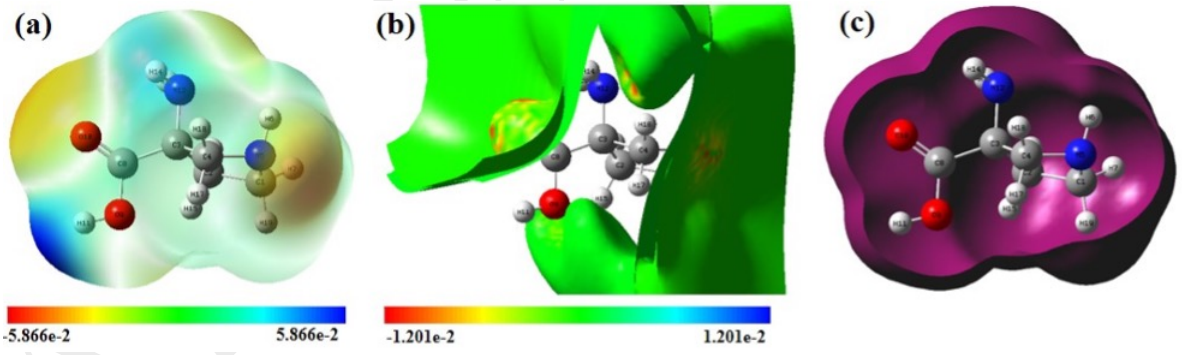

Figure 4. (a) Molecular electrostatic potential, (b) Electrostatic potential, and (c) Electron density of the Cucurbitine molecule.

Fig. 4(b) presents the ESP mapped onto an iso-density surface, ranging from -1.201×10^{-2} (red) to 1.201×10^{-2} a.u. (blue). It provides a visual depiction of reactive and chemically active sites, with blue regions indicating nucleophilic (electron-attracting) sites and red regions indicating electrophilic (electron-donating) sites. The electrophilic and nucleophilic sites in the ESP arise due to differences in electronegativity that create an uneven electron distribution. Oxygen and nitrogen, being electron-rich, act as nucleophilic sites, while hydrogen atoms, being electron-deficient, act as electrophilic sites. These sites mainly govern hydrogen bonding and intermolecular interactions [36–38].

Fig. 4(c) shows the ED distribution of the molecule. It illustrates the regions where electrons are most likely to be found. The smooth and continuous shape of this distribution indicates that the atoms are strongly bonded to each other, especially along the C–C, C–N, and C–O bonds. There is greater electron density near the more electronegative atoms, such as oxygen and nitrogen, because these atoms have a stronger tendency to attract electrons. Rather than showing a perfectly even charge distribution, the figure shows a balanced and continuous electron density with regions of higher concentration. This suggests effective orbital overlap and helps the molecule remain stable overall [39].

Density of states

Fig. 5 shows the DOS spectrum of the Cucurbitine molecule, which was calculated using the GaussSum 3.0 program [14]. DOS analysis provides insight into electron participation in the conduction and valence bands, as well as the degeneracy of energy levels [40]. Higher intensity indicates more available states at a specific energy, while zero intensity indicates that no states are available. In the DOS curve, occupied orbitals (green) represent electrons available for donation, whereas unoccupied orbitals (red) correspond to electron-accepting states [41]. The observed HOMO–LUMO gap from the DOS spectrum is 6.088 eV and is very close to the calculated HOMO–LUMO gap of 6.094 eV, confirming the consistency and accuracy of the electronic structure results. This agreement shows that the molecule has a large energy gap, indicating high stability, low reactivity, and insulating behavior. Thus, DOS analysis is important because it validates the orbital results and provides a clearer picture of electron distribution and possible electronic transitions.

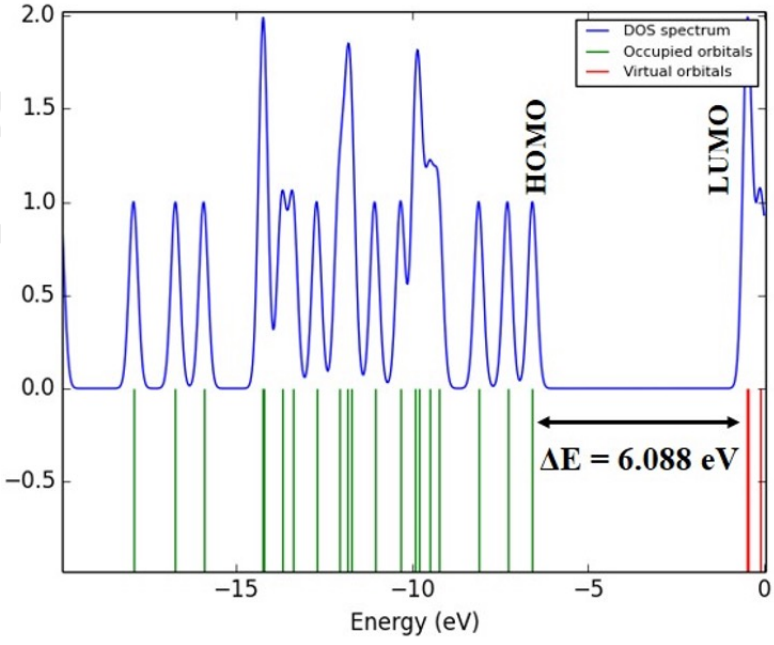

Figure 5. Density of states spectrum of the Cucurbitine molecule.

Mulliken atomic charge distribution

The Mulliken charge distribution shows how electrons are shared among atoms due to differences in electronegativity, leading to partial charge equalization within the molecule. It represents the electrostatic potential around the molecule and reflects bond polarity and chemical interactions. It is also related to molecular vibrations because electron distribution affects bond strength and atomic motion [42]. Fig. 6 shows the Mulliken atomic charge distribution, which reflects the impact of atomic displacement on the electronic structure, depending on the electron density. In Fig. 6, C3 exhibits the highest positive charge, whereas C4 exhibits the highest negative charge. The different Mulliken charges arise due to the unequal electron distribution caused by differences in electronegativity and the bonding environment. C3 is positive because it loses electron density to nearby atoms, while C4 is negative due to electron accumulation or resonance effects. Hydrogen atoms are mostly positive since electrons are drawn toward more electronegative atoms, whereas oxygen atoms are negative because they strongly attract electron density. This reflects bond polarity and helps identify reactive sites in the molecule.

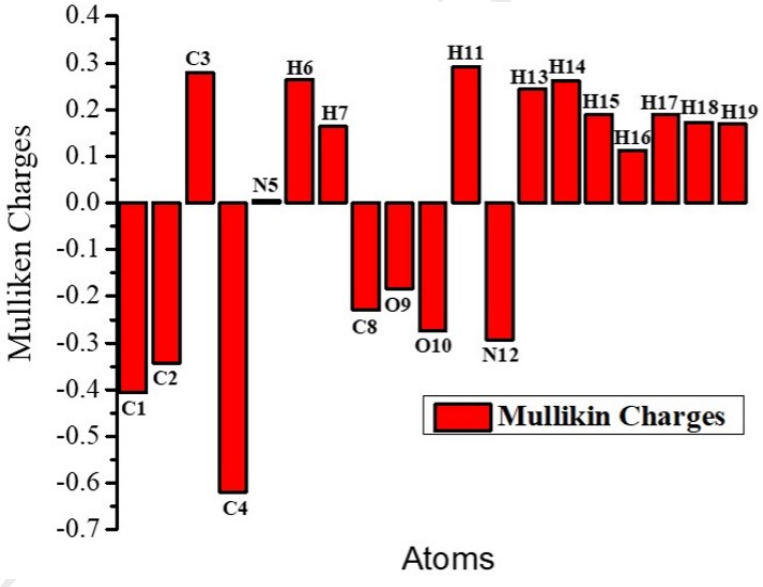

Figure 6. Histogram of the Mulliken atomic charge distribution for each atom in the Cucurbitine molecule.

Vibrational analysis

Vibrational analysis is an essential tool in molecular spectroscopy, dealing with the vibrational motions of atoms in a molecule. It is an important source of information about the molecular structure, bonding, stability, and spectroscopic behavior [26]. Fig. 7 presents the FT-IR spectrum of the Cucurbitine molecule. For a molecule containing N atoms, the total number of normal vibrational modes is given by $3N-6$ [43]. As Cucurbitine consists of 19 atoms, it exhibits 51 vibrational modes. Vibrational modes arise from the interaction between infrared radiation and the molecule, causing changes in the dipole

moment or polarizability, which determine whether a vibration is IR- or Raman-active [44, 45]. Analysis of the IR spectrum allows the identification of various molecular vibrations, including stretching and bending modes, as well as in-plane and out-of-plane motions. These results provide important insights into the dynamic behavior and structural characteristics of the Cucurbitine molecule.

C–C vibration

The C–C stretching vibration is expected to occur between 1625–1430 cm^{-1} in aromatic rings [26], whereas the typical C–C stretching mode is generally reported in the range of 1350–1420 cm^{-1}. The observed FT-IR peaks are located at 1345.17 and 1367.17 cm^{-1}. The reduced frequency of these modes is attributed to changes in the force constant and the vibrations of the molecule's functional groups. The theoretically predicted C–C vibrational frequencies obtained using the B3LYP/6-311++G(d,p) method are in excellent agreement with the experimental results.

C–H vibration

Aromatic C–H stretching vibrations are typically observed in the range of 3300–3000 cm^{-1} [46]. In the Cucurbitine molecule, these vibrations appear at 3035.73, 3049.36, 3061.94, 3095.18, and 3119.50 cm^{-1} in the FT-IR spectrum, consistent with the characteristic aromatic C–H stretching frequencies.

C–O vibration

The C–O single bond exhibits stretching vibrations in the range of 1300–1000 cm^{-1} [47]. The corresponding FT-IR band in the Cucurbitine molecule is observed at 1148.13 cm^{-1}. For the C=O functional group, the FT-IR spectrum shows a band at 1791.86 cm^{-1}, which is slightly higher than the reported stretching vibration range of 1643–1700 cm^{-1}. These vibrational assignments provide insight into the functional groups and confirm the structural features of the molecule.

C–N vibration

The C–N stretching vibration often occurs in a region where multiple bands can overlap, making precise assignment challenging. In the Cucurbitine molecule, the FT-IR spectrum shows a C–N stretching band at 1107.77 cm^{-1}, which lies within the predicted range of 1065–1397.8 cm^{-1} [48]. N–H stretching vibrations, characteristic of primary and secondary amines as well as amides, generally appear in the range of 3300–3500 cm^{-1} [30]. These vibrations agree well with the observed peaks at 3494.12, 3514.17, and 3564.49 cm^{-1}.

O–H vibration

The O–H vibration mode is weak because of intermolecular hydrogen bonding in the unassociated hydroxyl group (3580–3670 cm^{-1}) [49, 50]. The FT-IR spectrum of $C_5H_{10}N_2O_2$ shows an O–H vibration peak at 3756.83 cm^{-1}. The calculated vibration frequency agrees well with the standard value. The

relatively high wavenumber indicates that the O–H group experiences little or no hydrogen-bonding interaction, resulting in a stronger O–H bond and a higher stretching frequency. This observation confirms the presence of a free hydroxyl group and supports the proposed molecular structure.

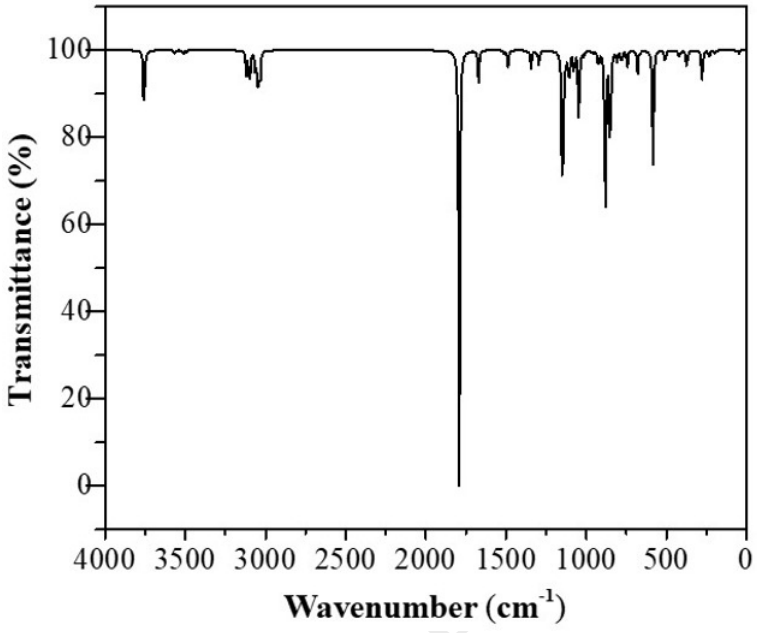

Figure 7. FT-IR spectrum of the Cucurbitine molecule.

Thermodynamic parameter analysis

The thermodynamic parameters include the specific heat capacity at constant volume (C_V), specific heat capacity at constant pressure (C_P), internal energy (U), enthalpy (H), entropy (S)), and Gibbs free energy (G). Fig. 8 illustrates the variation of these thermodynamic parameters over a temperature range of 10–500 K with increments of 10 K. As temperature increases, molecular vibrational motion intensifies, leading to systematic changes in these thermodynamic properties.

Fig. 8(a) shows that both C_V and C_P exhibit a gradual and nearly identical increase with increasing temperature. Similarly, the internal energy (U) and enthalpy (H), shown in Fig. 8(b), increase steadily with temperature and display comparable trends. Entropy (S), shown in Fig. 8(c), increases rapidly at lower temperatures, followed by a more gradual increase at higher temperatures.

In contrast, Gibbs free energy (G), shown in Fig. 8(d), decreases as temperature increases, consistent with its thermodynamic dependence on temperature and entropy. These changes occur because higher temperatures increase molecular motion and the accessibility of energy states. Consequently, U and H increase owing to greater molecular energy content, while C_V and C_P increase because additional vibrational modes contribute to the heat capacity. Entropy increases as disorder and the number of accessible microstates grow, with a more pronounced effect at lower temperatures. Gibbs free energy decreases

because the temperature–entropy term becomes increasingly dominant, favoring higher disorder [51].

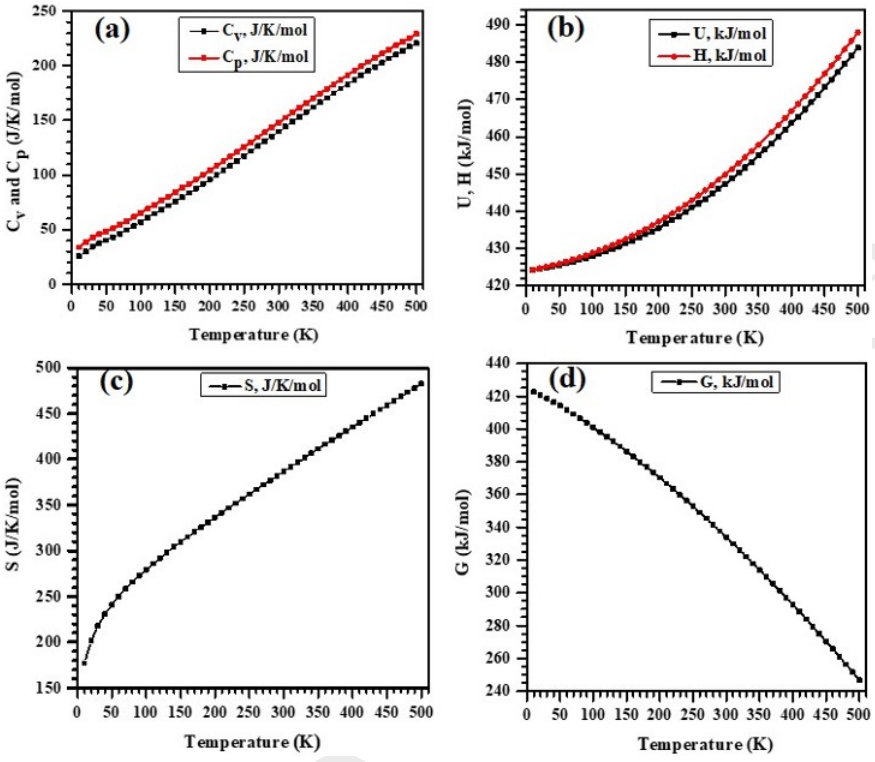

Figure 8. Variation of thermodynamic parameters with temperature: (a) Specific heat capacity at constant volume (C_V) and specific heat capacity at constant pressure (C_P), (b) Internal energy (U) and enthalpy (H), (c) Entropy (S), and (d) Gibbs free energy (G) of the Cucurbitine molecule.

These temperature-dependent trends provide important insight into the thermal stability and energetic behavior of Cucurbitine, confirming its predictable thermodynamic response across the investigated temperature range. Thermodynamic parameters such as heat capacity (C_P), entropy (S), and enthalpy (H), calculated within the physiologically relevant temperature range of 298–310 K, show smooth and predictable variations without abrupt changes, indicating thermodynamic stability under normal biological conditions. These observations are particularly relevant to the proposed biological and pharmaceutical significance of Cucurbitine, suggesting that the molecule can maintain its structural and energetic stability at temperatures corresponding to living systems.

IV. Conclusion

Density Functional Theory (DFT) calculations were performed to investigate the optimized geometry, electronic properties, spectroscopic characteristics, and thermodynamic parameters of the Cucurbitine molecule. Geometry optimization converged successfully after eight optimization cycles, yielding a final total energy of −456.64 Hartree (−12425.81 eV). This negative energy confirms that the molecule

attained a stable and well-converged minimum-energy configuration. The optimized structure provides a reliable basis for subsequent electronic and vibrational analyses.

The calculated energy gaps obtained from the DOS spectrum and the HOMO–LUMO analysis are 6.088 eV and 6.094 eV, respectively. The close agreement between these values confirms the internal consistency of the results. The relatively large energy gap indicates high kinetic stability and low chemical reactivity of the Cucurbitine molecule. Correspondingly, the global hardness and softness were calculated to be 3.047 eV and 0.329 eV, respectively, further supporting its stable nature.

The MEP and ESP surface maps reveal that oxygen and nitrogen atoms represent electron-rich regions that are susceptible to electrophilic attack, whereas hydrogen atoms correspond to electron-deficient regions prone to nucleophilic attack, suggesting potential sites for intermolecular interactions. The electron density (ED) analysis confirms the charge distribution within the molecule, highlighting electron delocalization and bonding characteristics. Mulliken charge analysis shows that the C3 atom carries the highest positive charge, whereas the C4 atom possesses the highest negative charge, identifying them as the most reactive sites for nucleophilic and electrophilic interactions, respectively.

The characteristic C–C stretching vibrations were observed in the range of 1350–1420 cm^{-1}, while the C–H stretching modes appeared at 3035.73, 3049.36, 3061.94, 3095.18, and 3119.50 cm^{-1}. The C=O stretching vibration was identified at 1791.86 cm^{-1}, C–N stretching vibrations at 1397.8 and 1065 cm^{-1}, and the O–H stretching vibration at 3756.83 cm^{-1}. These vibrational characteristics confirm the structural integrity of the Cucurbitine molecule and indicate its potential for intermolecular interactions, highlighting its relevance in biological and chemical applications.

The thermodynamic analysis indicates that all calculated thermodynamic parameters increase with increasing temperature, except for Gibbs free energy, which decreases because of its intrinsic dependence on temperature.

V. Acknowledgments

We gratefully acknowledge the Department of Physics, Patan Multiple Campus, Lalitpur, Tribhuvan University, Nepal and the Department of Physics, St. Xavier's College, Kathmandu, for their kind help and software facility support in this study.

References

[1] Kaushik U, Aeri V, Mir SR. Cucurbitacins—An Insight into Medicinal Leads from Nature. Pharmacognosy Reviews. 2015;9(17):12-8.

[2] Marie-Magdeleine C, Mahieu M, Archimede H. Pumpkin (Cucurbita moschata Duchesne ex Poir.)

Seeds as an Anthelmintic Agent? In: Preedy VR, Watson RR, Patel VB, editors. Nuts and Seeds in Health and Disease Prevention. Academic Press; 2011. p. 933-9.

[3] Varela C, Melim C, Neves BG, Sharifi-Rad J, Calina D, Mamurova A, et al. Cucurbitacins as Potential Anticancer Agents: New Insights on Molecular Mechanisms. Journal of Translational Medicine. 2022;20(1):630.

[4] Oukhrib R, Abdellaoui Y, Berisha A, Abou Oualid H, Halili J, Jusufi K, et al. DFT, Monte Carlo and Molecular Dynamics Simulations for the Prediction of Corrosion Inhibition Efficiency of Novel Pyrazolylnucleosides on Cu(111) Surface in Acidic Media. Scientific Reports. 2021;11(1):3771.

[5] Fernandez-Ochoa A, Leyva-Jimenez FJ, Cadiz-Gurrea MdlL, Pimentel-Moral S, Segura-Carretero A. The Role of High-Resolution Analytical Techniques in the Development of Functional Foods. International Journal of Molecular Sciences. 2021;22(6):3220.

[6] Sousa C, Moutinho CG, Carvalho M, Matos C, Vinha AF. Transforming By-Products into Functional Resources: The Potential of Cucurbitaceae Family Seeds in Cosmetics. Seeds. 2025;4(3):36.

[7] Salehi B, Capanoglu E, Adrar N, Catalkaya G, Shaheen S, Jaffer M, et al. Cucurbits Plants: A Key Emphasis to Its Pharmacological Potential. Molecules. 2019;24(10):1854.

[8] Armstrong L, Chang SL, Clements N, Hirani Z, Kimberly LB, Odoi-Adams K, et al. Molecular Recognition of Peptides and Proteins by Cucurbit[n]urils: Systems and Applications. Chemical Society Reviews. 2024;53(23):11519-56.

[9] Parr RG, Yang W. Density-Functional Theory of Atoms and Molecules. New York: Oxford University Press; 1989.

[10] Patrick GL. An Introduction to Medicinal Chemistry. 6th ed. Oxford University Press; 2017.

[11] Ge W, Chen X, Han F, Liu Z, Wang T, Wang M, et al. Synthesis of Cucurbitacin B Derivatives as Potential Anti-Hepatocellular Carcinoma Agents. Molecules. 2018;23(12):3345.

[12] Frisch MJ, et al.. Gaussian 09, Revision D.01; 2009. Gaussian, Inc., Wallingford, CT.

[13] Dennington R, Keith TA, Millam JM. GaussView Version 6; 2019. Semichem Inc. Shawnee Mission KS.

[14] Hachenberger D, Jungnickel D. Characters, Gauss Sums, and the DFT. In: Topics in Galois Fields; 2020. p. 489-533.

[15] Lu T, Chen F. Multiwfn: A Multifunctional Wavefunction Analyzer. Journal of Computational Chemistry. 2012;33(5):580-92.

[16] Humphrey W, Dalke A, Schulten K. VMD: Visual Molecular Dynamics. Journal of Molecular Graphics. 1996;14(1):33-8.

[17] Ignatov SK. Moltran, Version 2.5; 2004. N. I. Lobachevsky State University, Nizhny Novgorod, Russia.

[18] Koopmans T. Über die Zuordnung von Wellenfunktionen und Eigenwerten zu den Einzelnen Elek-

tronen Eines Atoms. Physica. 1934;1:104-13.

[19] Kaupp M, Danovich D, Shaik S. Chemistry Is about Energy and Its Changes: A Critique of Bond-Length/Bond-Strength Correlations. Coordination Chemistry Reviews. 2017;344:355-62.

[20] Ghimire R, Magar AR, Basnet B, Uprety R, Pudasainee K, Rai KB. Study of the Spectroscopic Analysis, Electronic Structure and Thermodynamic Properties of Ethylbenzene Using First-Principles Density Functional Theory. Contemporary Research: An Interdisciplinary Academic Journal. 2024;7(1):80-99.

[21] Rai KB, Teemilsina NK, Siwakoti B. First-Principles Study of Structural Equilibrium Configuration of Ortho-, Meta-, and Para-Chloroaniline Molecules. Scientific World. 2024;17(17):7-18.

[22] Fortenberry RC, Novak CM, Lee TJ, Bera PP, Rice JE. Identifying Molecular Structural Aromaticity for Hydrocarbon Classification. ACS Omega. 2018;3(11):16035-9.

[23] Ashraf A, Khalid M, Tahir MN, Yaqub M, Naseer MM, Kamal GM, et al. A Facile and Concise Route to (Hydroxybenzoyl)pyrido[2,3-*d*]pyrimidine Heterocycle Derivatives: Synthesis, and Structural, Spectral and Computational Exploration. RSC Advances. 2019;9(59):34567-80.

[24] Jezierska A. N–H...O versus O–H...O: Density Functional Calculation and First-Principles Molecular Dynamics Study on a Quinoline-2-Carboxamide N-Oxide. Journal of Molecular Modeling. 2015;21(3):47.

[25] Gannouni A, Tahri W, Roisnel T, Kefi R. X-Ray Diffraction and Computational Analysis of a Novel Hybrid Cu(II) Compound. Journal of Molecular Structure. 2023;1271:134094.

[26] Ojha T, Shrestha PM, Gupta SP, Rai KB. Quantum Chemical Insights into the Electronic, Vibrational and Thermodynamic Properties of Chloro-Substituted Anisole. Al-Nahrain Journal of Science. 2025;28(4):146-64.

[27] Megrouss Y, Salem Y, Mansour A, Benyahlou ZD, Kaas SA, Benaissi H, et al. Molecular Structure, Lattice Energy, Hirshfeld Surface and NCI-RDG Analysis, DFT Calculations, and In Silico Molecular Docking of an Imidazole Derivative. Physical Chemistry Research. 2024;12(4):975-90.

[28] Kumar PS, Vasudevan K, Prakasam A, Geetha M, Anbarasan PM. Quantum Chemistry Calculations of 3-Phenoxyphthalonitrile Dye Sensitizer for Solar Cells. Spectrochimica Acta Part A: Molecular and Biomolecular Spectroscopy. 2010;77(1):45-50.

[29] Uprety R, Ghimire R, Gharti Magar P, Rokka D, Khadka IB, Neupane R, et al. Study of the Molecular Structure, Electronic Structure, Spectroscopic Analysis and Thermodynamic Properties of Dibenzofuran Using First Principles. Journal of Nepal Physical Society. 2024;10(2):8-18.

[30] Basnet K, Neupane B, Gharti Magar P, Uprety R, Rai KB. A Computational DFT Insight into the Optimized Structure, Electronic Structures, Spectroscopic Analysis, and Thermodynamic Parameters of the Cytosine Molecule. Amrit Research Journal. 2024;5(1):140-50.

[31] Sabry NM, Badry R, Abdel-Gawad FK, Elhaes H, Ibrahim MA. Electronic Structure, Global Reac-

tivity Descriptors and Nonlinear Optical Properties of Glycine Interacted with ZnO, MgO and CaO for Bacterial Detection. Scientific Reports. 2024;14:22801.

[32] Shivaleela B, Shivraj GG, Hanagodi SM. Estimation of Dipole Moments by Solvatochromic Shift Method, Spectroscopic Analysis of UV–Visible, HOMO–LUMO, ESP Map, Mulliken Atomic Charges, NBO and NLO Properties of a Benzofuran Derivative. Results in Chemistry. 2023;6:101046.

[33] Rai KB, Khadka IB, Koirala AR, Ray SK. Insight into Cleaning, Doping and Defective Effects on the Graphene Surface Using Methanol. Advances in Materials Research. 2021;10(4):283-92.

[34] Singh JS, Khan MS, Uddin S. A DFT Study of Vibrational Spectra of 5-Chlorouracil with Molecular Structure, HOMO–LUMO, MEP/ESP and Thermodynamic Properties. Polymer Bulletin. 2023;80(3):3055-83.

[35] Gharti Magar P, Uprety R, Rai KB. First-Principles DFT Study of the Molecular Structure, Spectroscopic Analysis, Electronic Structures and Thermodynamic Properties of Ascorbic Acid. Himalayan Physics. 2024;11(1):28-40.

[36] Prasana JC, Muthu S, Abraham CS. Molecular Docking Studies, Charge-Transfer Excitation and Wavefunction Analyses (ESP, ELF, LOL) on Valacyclovir: A Potential Antiviral Drug. Computational Biology and Chemistry. 2019;78:9-17.

[37] Basavaraj S, Gounhalli SG, Patil O, Hanagodimath SM. Quenching of Fluorescence, Dipole Moments and DFT Studies of a Newly Synthesized Aminothiadiazole Coumarin Derivative. Journal of the Maharaja Sayajirao University of Baroda. 2021;55(1):200-18.

[38] Yankova R, Genieva S, Halachev N, Dimitrova G. Molecular Structure, Vibrational Spectra, MEP, HOMO–LUMO and NBO Analysis of Hf(SeO3)(SeO4)(H2O)4. Journal of Molecular Structure. 2016;1106:82-8.

[39] Thapa D, Rai KB, Pandey B, Ghimire MP. Molecular Insights into Herniarin: Structural, Spectroscopic, Electronic and Thermodynamic Characterization via Density Functional Theory. Himalayan Physics. 2025;12(1):64-83.

[40] Ghafoor S, Mansha A, Asim S, Usman M, Zahoor AF, Ali HS. Structural, Spectral, Frontier Molecular Orbital and Thermodynamic Analysis of 2-Hydroxy-2-Methylpropiophenone by MP2 and B3LYP Methods. Journal of Theoretical and Computational Chemistry. 2020;19(5):2050020.

[41] Rai KB, Khadka IB, Kim EH, Ahn SJ, Kim HW, Ahn JR. Influence of Hydrophobicity on the Chemical Treatments of Graphene. Journal of the Korean Physical Society. 2018;72(1):107-10.

[42] Govindasamy P, Gunasekaran S, Srinivasan S. Molecular Geometry, Conformational, Vibrational Spectroscopic, Molecular Orbital and Mulliken Charge Analysis of 2-Acetoxybenzoic Acid. Spectrochimica Acta Part A: Molecular and Biomolecular Spectroscopy. 2014;130:329-36.

[43] Bisong EA, Louis H, Unimuke TO, Odey JO, Ubana EI, Edim MM, et al. Vibrational, Electronic, Spectroscopic Properties, and NBO Analysis of *p*-Xylene and Halogenated *p*-Xylenes: A DFT Study.

Heliyon. 2020;6(12):e05783.

[44] Khadka IB, Rai KB, Rokka D. Low-Power Light-Irradiation-Based Plasmonic Photoresponse on a Quasi-Freestanding Monolayer/AuNPs Hybrid System. Indian Journal of Physics. 2025;99:95-103.

[45] Khadka IB, Rai KB, Alsardia MM, Haq BU, Kim SH. Raman Investigation of Substrate-Induced Strain in Epitaxially Grown Graphene on Low/High Miscut-Angled Silicon Carbide and Its Application Perspectives. Optical Materials. 2023;140:113836.

[46] Sebek J, Knaanie R, Albee B, Potma EO, Gerber RB. Spectroscopy of the C–H Stretching Vibrational Band in Selected Organic Molecules. The Journal of Physical Chemistry A. 2013;117(32):7442-52.

[47] Seshadri S, Rasheed MP. Molecular Structure, Vibrational, UV, NMR, Molecular Electrostatic Surface Potential and HOMO–LUMO Analysis of 1,4-Dichloro-2-Nitrobenzene. International Journal of Engineering and Science. 2016;6(4):6-18.

[48] Bishwokarma N, Budha C, Teemilsina NK, Rai KB. Exploring Vibrational Spectra, Electronic Properties and Thermal Analysis of the Isoguanine Molecule Using DFT. Scientific World. 2025;18(18):5-14.

[49] Arjunan V, Balamourougane PS, Govindaraja ST, Mohan S. A Comparative Study on the Vibrational, Conformational and Electronic Structure of 2-(Hydroxymethyl)pyridine and 3-(Hydroxymethyl)pyridine. Journal of Molecular Structure. 2012;1018:156-70.

[50] Baranska M, Roman M, Majzner K. General Overview on Vibrational Spectroscopy Applied in Biology and Medicine. In: Optical Spectroscopy and Computational Methods in Biology and Medicine. Dordrecht: Springer; 2014. p. 3-14.

[51] Basnet B, Rana Magar A, Ghimire R, Joshi U, Rai KB. First-Principles Calculations to Investigate Structural, Spectroscopic Features, Electronic and Thermodynamic Properties of Trichloroacetaldehyde. Himalayan Journal of Science and Technology. 2024;8(1):1-9.